Low temperature growth of graphitic carbon on porous silicon for high-capacity lithium energy storage

Xiang Han [a,b,**], Ziqi Zhang [b], Songyan Chen [b,*], Yong Yang [c]

[a] College of Materials Science and Engineering, Nanjing Forestry University, Nanjing, 210037, China
[b] Department of Physics, Xiamen University, Xiamen, 361005, China
[c] State Key Laboratory for Physical Chemistry of Solid Surfaces, Department of Chemistry, Xiamen University, Xiamen, 361005, China

HIGHLIGHTS

- Thin graphitic carbon is in-situ grown at 700 °C with Al_2O_3 catalyst.
- The graphitic carbon enhances solid electrolyte interphase and particle integrity.
- The silicon/graphitic carbon delivers an accumulated capacity of 492 mAh cm^{-2}.

ARTICLE INFO

ABSTRACT

With highly yield and low-cost micrometer-sized polycrystalline silicon powders, a hierarchical porous silicon (PS) structure is fabricated. As a novel passivated layer, graphitic carbon (GC) is in-situ growth on the three-dimensional surfaces of PS. The GC is synthesized with 1 nm Al_2O_3 catalyst, and the thickness can be controlled to 2 nm at a relatively low temperature 700 °C. With this unique GC layer coated PS, the structure integrity and solid electrolyte interphase stability substantially improved. As a result, the PS/GC shows a high capacity retention of 91% after 100 cycles at 0.2 A g^{-1}. During a long-life test at 1 A g^{-1}, the PS/GC electrode delivers 1024 mAh g^{-1} after 600 cycles. In addition, an accumulated areal capacity of 492 mAh cm^{-2} is achieved, further demonstrates the high mass loading of micrometer-sized PS as well as the electrochemical stability of highly-stacking GC coating layer. Our work invents a new approach of the GC growth and its application on large volume change electrode materials, which is enabled by a low temperature Al_2O_3 catalyzed method.

1. Introduction

We are on the long way to further reduce carbon dioxide emission and to use green energy such as solar and wind energy. On the other hand, the wide usage of portable electronics, electric vehicles have shown great demand for high energy Li-based energy storage systems [1, 2]. One of the key enabling methods is designing high capacity electrode materials, such as Si, Ge and Sn anodes [3]. Among them, Si is a promising candidate due to the highest specific capacity of ~3579 mAh g^{-1} ($Li_{15}Si_4$), earth abundant and environmental friendly nature [4,5]. However, the cycling performance of Si-based anodes in lithium batteries is far below commercial criteria due to its large volume expansion (~300%), which causes particles fracture, loss of electronic contact and unstable solid-electrolyte interphase (SEI) [6,7]. Nanometer Si and

amorphous carbon (aC) composite material is one of the most attractive strategies to address the above-mentioned issues [8–14]. The advantages of the unique structure are obvious: (1) the aC shells reduce the direct exposure of Si to the electrolyte and enhance the SEI stability; and (2) the carbon shells are electrically conductive, providing essential electron transportation to the inner Si. However, for nanometer Si, due to its intrinsic high specific surface area, usually shows low tap density and low volumetric capacity. In addition, the amorphous carbon with defects and mesopores is easily react with liquid electrolyte, leading to low Coulombic efficiency. Regarding this, highly-yield and low-cost micrometer-sized Si should be used to improve the tap density. Graphitic carbon (GC) is promising to further reduce electrolyte decomposition the due to its highly crystalline nature. The growth of GC was normally at 900–1100 °C [15–17], which induces severe reaction
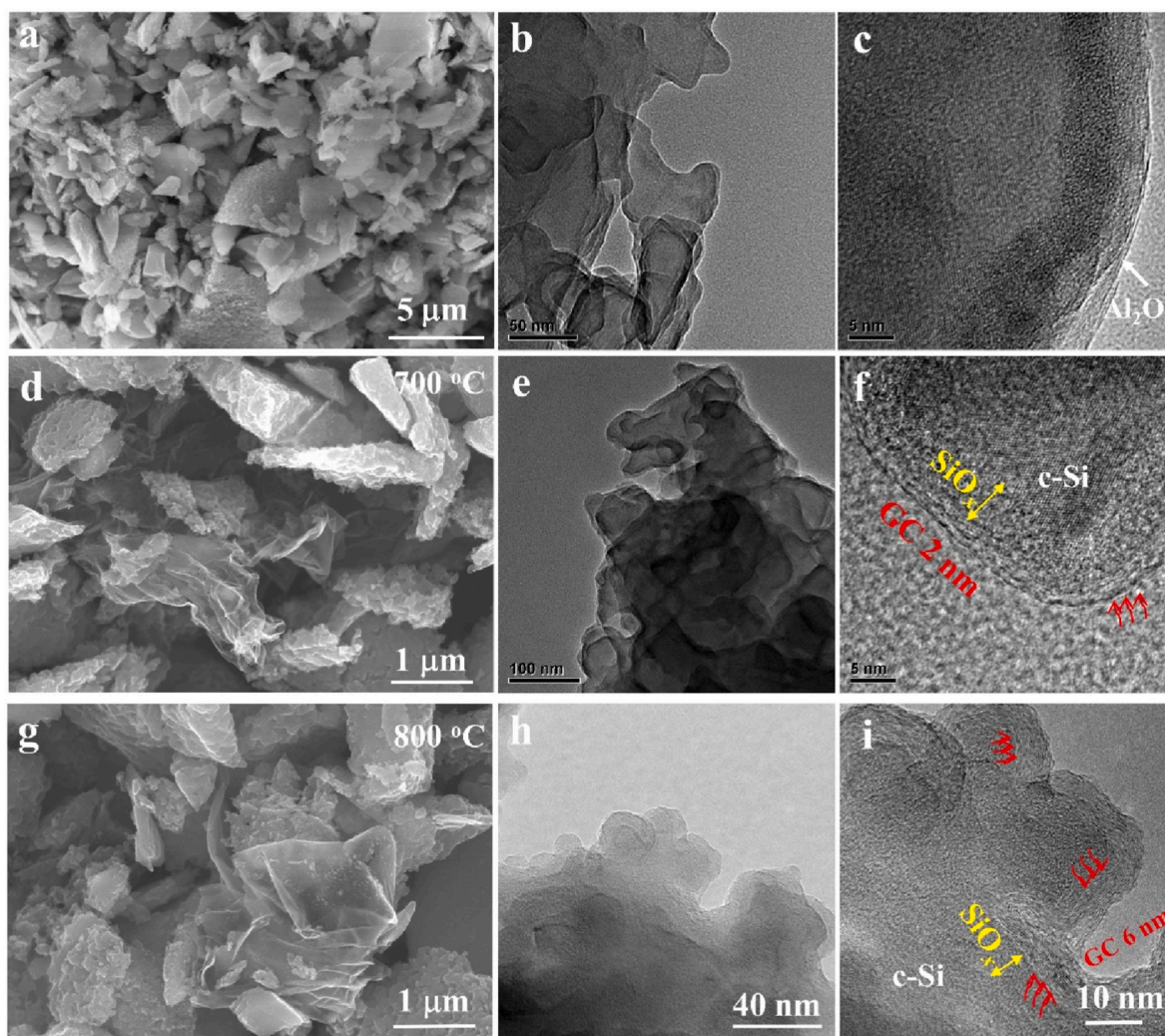
Fig. 1. (a) SEM image of a separate PS particle with Al_2O_3 coating layer. (b) TEM image of a separate PS particle with Al_2O_3 coating layer. (c) High resolution TEM image of PS particle with Al_2O_3. (d) SEM image of PS/GC grown at 700 °C. (e) TEM image of PS/GC grown at 700 °C. (f) High resolution TEM image of PS/GC grown at 700 °C. (g) SEM image of PS/GC grown at 800 °C. (h) TEM image of PS/GC grown at 800 °C. (i) High resolution TEM image of PS/GC grown at 800 °C.

between Si and carbon and forms insulated SiC layer.

Herein, we develop novel porous silicon (PS) and GC carbon composite at a relatively low temperature (700 °C). The growth of the GC layer is enabled by Al_2O_3-assisted chemical vapor deposition (CVD) technique with ethanol as precursor. The ultra-thin GC with a thickness of 2 nm shows highly stable electrolyte resistance. Because the thickness is only 2 nm, it has high kinetics for both electrons and Li ions. In addition, due to oxidation nature of ethanol, a 4 nm SiO_2 is in-situ formed during the CVD process. The SiO_2 layer helps to release the stress during volume change, which helps to improves the PS particle integrity. As a result, the stability of particle structure and SEI significantly enhanced by the well-designed SiO_2/GC coating layer. Tested in lithium cells, the PS/GC anodes shows stable cycling performance at low specific current of 0.2 A/g with a wide voltage range of 0.005–2.5 V. Even at a high rate of 1 A g^{-1}, the PS/GC anode exhibits a capacity of 1000 mAh g^{-1} after 600 cycles, thus an accumulated areal capacity of 600 mAh cm^{-2} achieved. Our GC coating technique provides a promising approach to address the structure and electrochemical instability associated with large volume change electrode materials. The low temperature CVD process is also friendly to energy consuming.

2. Experimental section

2.1. Materials synthesis

With micrometer-sized polycrystalline silicon particles (~1.5 μm), porous silicon (PS) particles were fabricated using a wet etching method. The etching electrolyte contains 25 mM $CuSO_4$+5 M hydrofluoric acid (HF). The silicon particles were immersed and stirred in this electrolyte at 55 °C for 12 h. The obtained PS particles were then completely treated with concentrated nitric acid at 25 °C for 2 h to dissolve residual Cu. Before graphitic carbon growth, 1 nm Al_2O_3 was coated on the surface of PS by atomic layer deposition (ALD, Picosun R-200 Advanced) technique at 70 °C. The precursors are trimethyl aluminium (TMA) and H_2O. The obtained PS/Al_2O_3 particles were then transferred into a chemical vapor deposition chamber and heated to 700 °C or 800 °C at a rate of 10 °C min^{-1} under argon (200 sccm) bubbled ethanol steam and kept for 2 h, then cooled naturally.

2.2. Characterization

The morphology of PS/GC was characterized by scanning electron microscope (SEM, Hitachi S4800) and transmission electron microscope (TEM, Tecnai F30). Powders X-ray diffraction (Rigaku Ultima IV) was used to test the crystalline structure of PS/GC particles with an
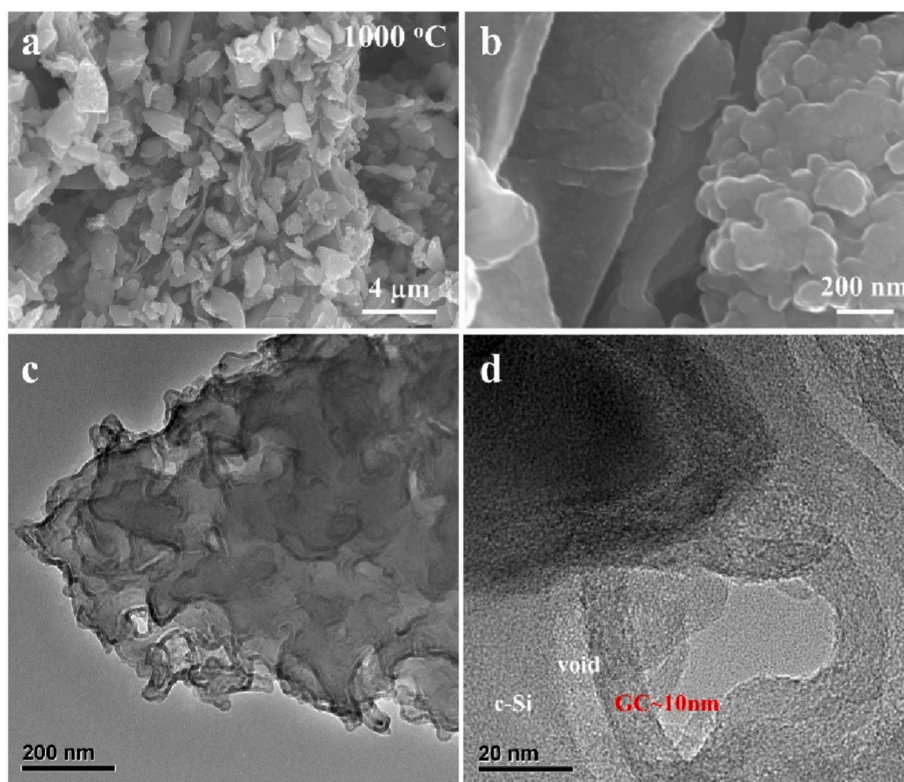
Fig. 2. (a) SEM image of PS/GC grown at 1000 °C. (b) High resolution SEM image of PS/GC grown at 1000 °C. (c) TEM image of PS/GC grown at 1000 °C after HF etching. (d) High resolution TEM image of PS/GC grown at 1000 °C after HF etching.

accelerating voltage of 15 KV. The Raman spectrum was tested on a WITEC system with a laser wavelength of 532 nm. A Nicolet380 FTIR equipment was used to acquire the transmittance spectrum in a wavenumber range of 400–4000 cm^{-1}.

2.3. Electrochemical evaluation

To evaluate the electrochemical performance, PS/GC and PAN (1:1 wt%) solution were mixed into slurry and blade casted on copper foil. Then the as-casted electrodes were annealed at 700 °C for 6 h under high purity argon (99.999%) to get PS/GC@c-PAN electrodes. After heat treatment, the amount of carbon and Si were 25 wt% and 75 wt%, respectively. The total mass loading is ~0.8 mg cm^{-2}. The PS/GC@c-PAN electrodes were directly assembled using CR2032 coin cell with lithium counter electrodes in a glovebox (Mbraun, H_2O, $O_2 < 0.5$ ppm). The electrolyte was 1 M $LiPF_6$ in ethylene carbonate (EC), dimethylcarbonate (DMC) and diethylcarbonate (DEC) (1:1:1 by volume) with 10% fluorinated ethylene carbonate (FEC) additive. The mass loading was weighed with a microbalance (METTLER TOLEDO XS3DU). A The galvanostatic cycling was tested using NEWARE CT-4000 (mA) system between 0.005 V and 2.5 V at 30 °C. The impedance spectroscopy (VersaSTAT MC, America) was tested from 100 kHz to 10 mHz under AC stimulus with an amplitude of 10 mV.

3. Results and discussion

Before GC coating, the SEM and TEM images of Al_2O_3 coated PS is shown in Fig. 1(a) and (b), a uniform layer is completely coated on its surfaces and pores in a smooth nature. In a high magnification (Fig. 1c), the coating layer exhibits amorphous characteristic and adhesives on the surface of crystalline Si. To track the morphology evolution and to reveal the effects of Al_2O_3 layer on the growth of GC, scanning electron microscope (SEM) images and transmission electron microscope (TEM) images of PS/GC grown at 700 °C and 800 °C are provided. In Fig. 1d,

after grown in 700 °C for 2 h, the micrometer-sized PS particles are uniformly coated with GC. The well-aligned nanoscale pores are clear observed after GC coating, implying the GC grown along the pore walls. Because the Al_2O_3 was directly deposited on porous silicon (PS) powders via an ALD method. It is known that some particles are aggregated in where large area Al_2O_3 film deposited. As a result, some flexible and large areal GC nanosheet are found in the inter-particle space. In the TEM image (Fig. 1e), the pores show layer-stacking structure with uniform GC layer coated. The three-dimensional (3D) GC completely coated all the inner pores. Note that the Al_2O_3 layer was deposited by ALD, should be 3D coated. The interconnected 3D GC could provide fast Li ions and electrons through the whole PS. High resolution TEM (HRTEM) was used to analysis the interfacial layer between GC and inner Si. From Fig. 1f, the thickness of GC layer is calibrated to be 2 nm while inner Si remains pristine crystalline nature. An amorphous interphase layer with a thickness of ~4 nm was in-situ formed during GC growth. Considering the weak oxidation property of ethanol, the amorphous layer may be SiO_x. At the growth temperature of 700 °C, the thickness remains at 2 nm even after 2 h. Increase the growth temperature to 800 °C, the thickness of GC enhances while the pores are still could be observed (Fig. 1g). The uniform GC coating layer was found to be ~6 nm (Fig. 1h). In the HRTEM image (Fig. 1i), the GC shows highly crystalline nature, onion-like stacking structure was clearly observed, which is further confirmed by its FFT patterns (Fig. S1). The inter-plane distance is calibrated to 0.34 nm. And the amorphous SiO_x thickness increased to 6 nm. The carbon contents of PS/GC grown after 700 °C and 800 °C are 5.67 wt% and 11.45 wt%, respectively (Fig. S2).

Further increase the growth temperature to 1000 °C, all PS particles coated by thick GC and their pores are filled (Fig. 2a,b). To demonstrate the SiO_x nature of the amorphous interphase, the PS/GC particles were treated with hydrofluoric acid (HF). After etching, uniform void space formed between crystalline Si and GC (Fig. 2c). It is clear that GC rings in-situ growth inner the pores, implying its completely coating nature prepared by CVD method. The FFT pattern shows a corresponding circle
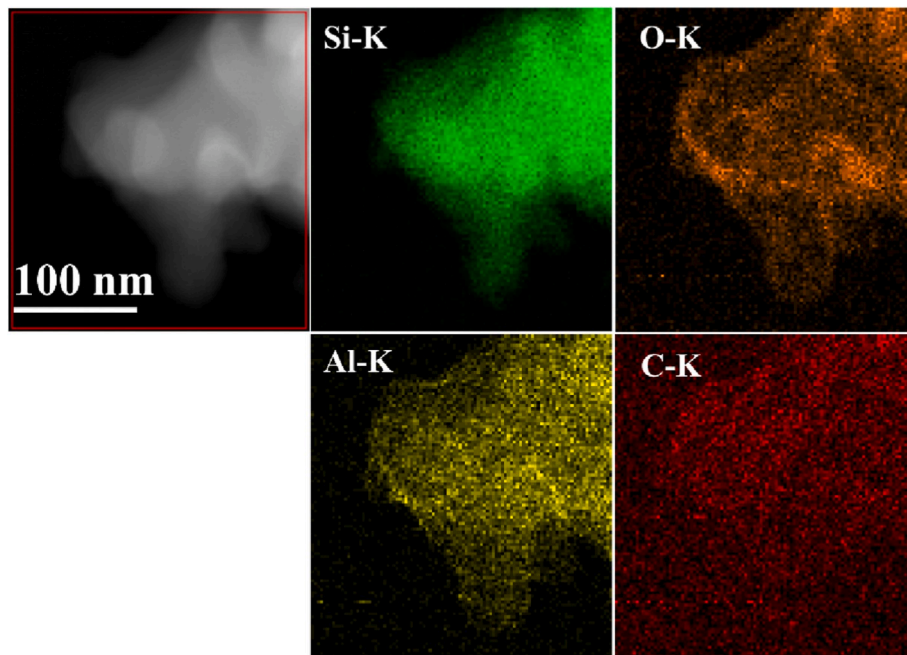
Fig. 3. Dark-filed TEM image of PS/GC grown at 700 °C and corresponding EDS elemental mapping.
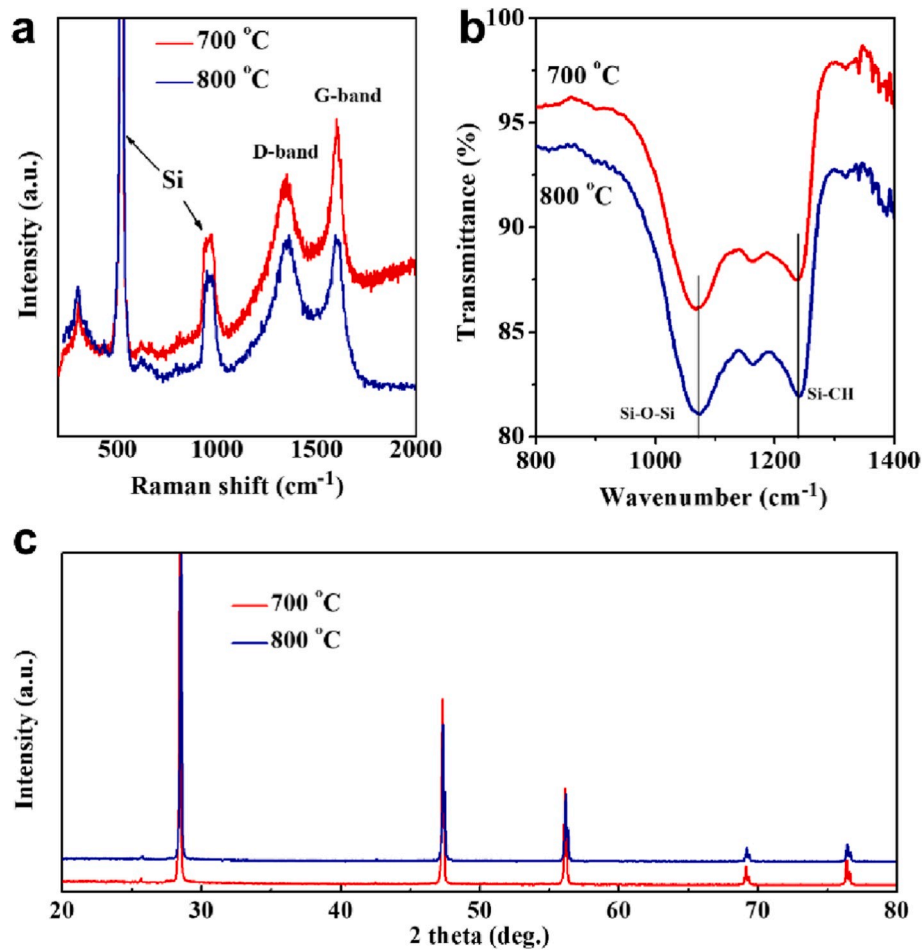

Fig. 4. (a) Raman spectrum of PS/GC grown at 700 °C and 800 °C. (b) FTIR spectrum of PS/GC grown at 700 °C and 800 °C. (c) XRD patterns of PS/GC grown at 700 °C and 800 °C.
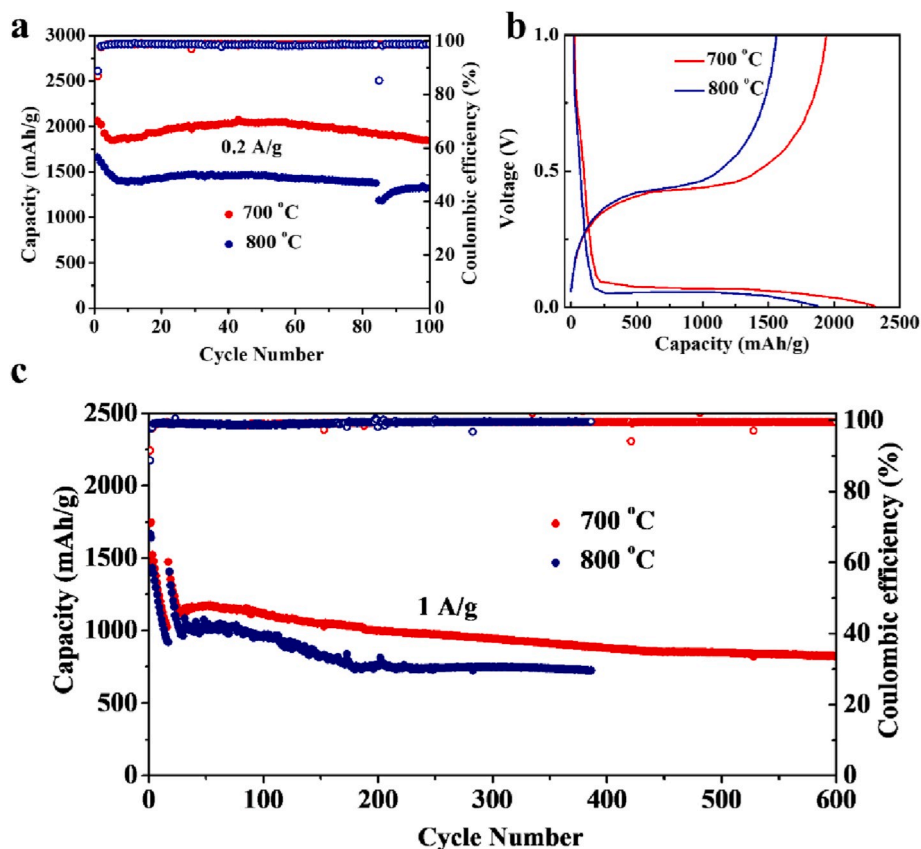
Fig. 5. (a) Galvanic cycling performance of PS/GC grown at 700 °C and 800 °C. (b) Voltage profiles of PS/GC grown at 700 °C and 800 °C. (c) Long-term cycling performance of PS/GC grown at 700 °C and 800 °C.

shape (Fig. S1). In high resolution TEM image (Fig. 2d), the thickness of void space and GC are 10 nm and 10 nm, respectively. The thickness of GC and amorphous SiO_x is dependent on the growth temperature, implying the growth mechanism is not simply physical stacking carbon atoms layer by layer. Instead it should be correlated to catalyzed effect of Al_2O_3 on the substrate. There is an interfacial carbon layer, which has a graphene-like honeycomb lattice and is covalently bonded to the Al_2O_3 substrate. The ethanol could in-situ oxide the Si into amorphous SiO_x during GC growth process.

To further analysis the chemical elements of PS/GC and its interphase, we carried out energy dispersive spectroscopy (EDS) mapping. As shown in the dark field TEM image (Fig. 3), the PS/GC shows clear hierarchical interconnected structure. From the EDS elemental mapping, the inner skeleton corresponds to Si signal, while the carbon signal shows a uniform distribution across the whole particle. The O signal fits the inter-parts between Si and carbon and the Al just adheres to the carbon. The EDS mapping further confirms the GC/SiO_x coating layer on PS while the GC is grown with Al_2O_3 assisted method. The GC is expected to stabilize the interphase with liquid electrolyte due to its highly crystalline nature. As we know that GC shows a low lithium ions diffusion coefficient, its thickness should be thin enough to enable fast lithium ion transportation. The SiO_x was demonstrated to release the stress during volume expansion in a proper thickness range between 4 and 7 nm. As a result, a multifunctional is fabricated GC/SiO_x in one step CVD process at a relatively low temperature between 700 and 800 °C.

To characterize the chemical structure of PS/GC, we have carried out Raman of FTIR spectra. As shown in Fig. 4a, the peaks at 516 and 960 cm^{-1} are attributed to the vibration of Si–Si bond [18]. The sharper G band (1600 cm^{-1}) originates from highly ordered plane vibration of the sp^2-carbon atoms in two-dimensional lattice and is a doubly degenerate (TO and LO) phonon mode (E_{2g} symmetry) at the Brillouin zone center

[19–21]. The position of G band is 1580 cm-1 for graphene grown on SiO_2 (300 nm)/Si. The significant blueshift (20 cm^{-1}) of the G band can be understood by the strain effect with Al_2O_3 substrate. Between GC and the Al_2O_3 substrate, there is an interfacial carbon layer, which has a graphene-like honeycomb lattice and is covalently bonded to the Al_2O_3 substrate [22]. This will change the lattice constant as well as the electronic properties of the substrate. Therefore, the lattice mismatch between the graphene lattice and interfacial carbon layer may cause a compressive stress on GC, giving rise to the shift in the Raman G band peak frequencies. The interfacial carbon layer adsorbed on the Al_2O_3 layer originates from the decomposition process of ethanol into ethene. Al_2O_3 serves as catalyst to the dehydration reaction occurs through an E2-elimination mechanism involving either surface O and/or OH groups of the oxides at around 350 °C [23]. Further increase growth temperature to 700 °C, ethene decompose into the interfacial layer adsorbed on the Al_2O_3. The pronounced D band (1350 cm^{-1}) with a narrow bandwidth suggests that some defects are present to facilitate Li-ion transport. The intensity ratio of D band to G band represents the degree of graphite.

During the dehydration process of ethanol, the by-product H_2O has oxidability thus reacts with Si to in-situ form SiO_x. FTIR was carried out to analyse the chemical valence of Si–O bond. As shown in Fig. 4b, an adsorption peak at 1080 cm^{-1} was observed in both PS/GC grown at 700 °C and 800 °C samples, which originates from the Si–O stretch (TO) vibration [24]. Pai have suggested that Si–O–Si stretching frequency scales linearly with oxygen concentration and obeys the following equation: x = (Si–O–Si stretching frequency-932)/68 [25]. According to this equation, the x of SiO_x in PS/GC is 2. The peak located at 1250 cm^{-1} is associated with Si–CH deformation vibration [25], which further confirms the interfacial carbon layer. The GC growth process in a CVD chamber does not change the crystalline nature of inner Si, as shown in

Table 1
Growth temperature, thickness of GC coated Si anodes and their electrochemical performance.

Temperature/$^{\circ}$C	Thickness/ nm	Accumulated capacity/mAh cm^{-2}	References
450	5	392	[29]
450	5	96	[30]
900	2	90	[31]
1050	8	220	[15]
950	2	386	[32]
950	3	520	[33]
1000	2	200	[16]
950	10	160	[17]
700	2	492	This work

Fig. 4c, the PS shows typical cubic Si X-ray diffraction (XRD) patterns after 700 °C or 800 °C [26].

Half cells with Li metal counter electrodes were fabricated to evaluate the effects of GC/SiO$_x$ on the electrochemical performance of PS/GC electrodes. The specific capacity is calculated on the total mass of the PS, SiO$_x$, Al$_2$O$_3$ and GC. The average mass loading is 0.8 mg cm^{-2} and all cells were tested between 0.005 and 2.5 V vs. Li/Li$^+$. In Fig. 5a, the electrode of PS/GC grown at 700 °C (named PS/GC-700) exhibits an initial reversible capacity of 2062 mAh g^{-1} with a Coulombic efficiency at 86.8%. At the specific current of 0.2 A g^{-1}, the specific capacity decreased to 1860 mAh g^{-1} at the 10th cycle. Laterally, the specific capacity increased slowly from 10th to 60th cycle with a value of 2022 mAh g^{-1}. The capacity increasement is associated with the kinetics. Because SiO$_x$ is electron insulated and has low lithium ion coefficient until it turns into lithium ion conductor LiSiO$_x$ [27]. During this lithiation process, the kinetics enhances and accordingly lower the polarization voltage. Even after 100 cycles, the specific capacity remains at 1842 mAh g^{-1}, 91% retention of the first cycle. For the PS/GC-800 electrode, the initial capacity is lower than that of PS/GC-700, a

capacity of 1660 mAh g^{-1} was achieved with a capacity retention of 1323 mAh g^{-1} after 100 cycles. The lower capacity is associated with large polarization voltage caused by thick GC/SiO$_x$ layer. As a result, the initial capacity of PS/GC-100 is only 1350 mAh g^{-1} and retains 1128 mAh g^{-1} after 100 cycles (Fig. S3). This assumption is confirmed by the lithiation potential comparison in Fig. 5b, the pleatue of PS/GC-700 locates at 70 mV while PS/GC-800 shows the pleatue at 55 mV. It is reported that crystalline Si exhibits a plateau at 100 mV vs. Li/Li$^+$ associated with the Si–Si bond [28]. So, the activation energy of GC/SiO$_x$-700 is about 30 meV, and that 45 meV of GC/SiO$_x$-800. With this unique temperature dependent CVD growth technique, 2 nm GC and 4 nm SiO$_x$ was successfully fabricated, the thin GC/SiO$_x$ helps to enhance the cycling performance with high lithium ion and electron conduction kinetics. Even at a high specific current rate of 1 A g^{-1}, a stable cycling performance was obtained after a quick fading during the initial 20 cycles (Fig. 5c). The PS/GC-700 electrode exhibits a capacity of 1024 mAh g^{-1} after 600 cycles. We also tested the long-term cycling data of PS/GC grown at 800 °C, which shows a similar trend. The specific capacity is about 150 mAh/g lower than that of PS/GC grown at 700 °C, due to its large polarization voltage. The excellent cycling performance can be attributed to the following reasons: (1) the hierarchical porous structure enhances the particle integrity, the inner pores accommodate volume change during lithium insertion and extraction while the silicon skeleton keep interconnected; (2) The GC/SiO$_2$ coating layer not only further release the stress during volume expansion but also stabilize the interphase with liquid electrolyte.

The ultra-thin 2 nm GC layer grown at a low temperature of 700 °C significantly enhances the particle structure and SEI stability of PS. In addition, micrometer-sized PS anode works over 600 cycles at a mass loading of 0.8 mg cm^{-2} (Fig. 5c). Accumulated areal capacity during the whole life is crucial parameter of a cell. By comparison, we have summarized the growth temperature and thickness of GC coated Si anodes, and their accumulated capacity performance in Table 1. With nickel as
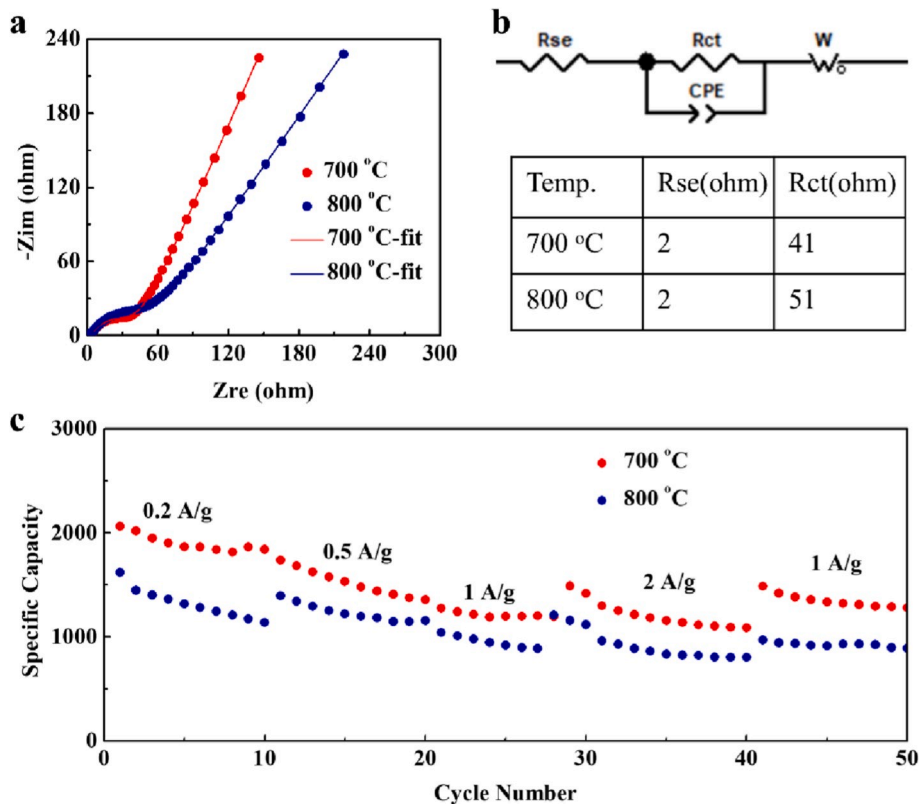

Fig. 6. (a) The impedance spectroscopy and fitting curves of PS/GC grown at 700 °C and 800 °C. (b) The equivalent circuit and corresponding fitting results of the SEI resistance (Rse) and charge transfer resistance (Rct). (c) Rate performance of PS/GC grown at 700 °C and 800 °C.

catalyst, the growth temperature can be low as 450 °C with a thickness of ~5 nm. With nickel catalyzed growth of GC, the micrometer-sized anode (3 μm) delivers an accumulated capacity of 392 mAh cm^{-2}, while nano-Si shows a value at 96 mAh cm^{-2}. Without nickel catalyst, the growth temperature of GC is normally between 900 °C and 1050 °C, the thickness ranges from 2 nm to 10 nm. The accumulated areal capacities are in a range of 100–500 mAh cm^{-2}. In this work, for the first time, the growth temperature can be at 700 °C with Al_2O_3 as catalyst. With an ultra-thin 2 nm GC, the well-designed micrometer-sized PS exhibits an accumulated capacity of 492 mAh cm^{-2}. The electrochemical performance is one of the best results reported so far, which further demonstrate the superiority of the GC coating layer and micrometer-size PS structure.

To reveal the reasons to the high kinetics of PS/GC grown at 700 °C, impedance (EIS) was carried out. As shown in Fig. 6a, based on the equivalent circuit, the fitting curves are in well consistence with the original data. From the fitting results in Fig. 6b, the charge transfer resistance of PS/GC grown at 700 °C (41Ω) is smaller than that grown at 800 °C (51 Ω). It is well known that at least two electrochemical processes related with charge transfer resistance: lithium ion redox; and transportation at the interphase [34]. Herein, the thin SiO_x/GC layer contributes to fast lithium ions transportation. As a result, the PS/GC grown at 700 °C exhibits better rate performance (Fig. 6c), For example, the specific capacities (the last cycle of each current) at 2 A g^{-1} and 1 A g^{-1} are 1087 mAh g^{-1} and 1281 mAh g^{-1}, respectively. While the PS/GC grown at 800 °C delivers 804 mAh g^{-1} and 892 mAh g^{-1} at 2 A g^{-1} and 1 A g^{-1}, respectively.

4. Conclusion

In summary, to solve the particle fracture and unstable SEI issues during repeated volume changes, a unique GC layer is in-situ grown on the surface of PS with Al_2O_3 catalyst. The growth temperature is decreased to 700 °C and the thickness can be controlled at 2 nm. With the well-designed GC/Al_2O_3 layer, the PS anode shows a high capacity retention of 91% after 100 cycles at 0.2 A g^{-1}. During a long-life test at 1 A g^{-1}, the PS/GC electrode delivers 1024 mAh g^{-1} after 600 cycles. More importantly, an accumulated areal capacity of 492 mAh cm^{-2} is achieved. The superior performance is attributed to the high crystalline GC coating layer and hierarchical porous structure, which substantially improve the SEI stability and structure integrity. Our work shed light on the way to design ultra-thin GC layer at low temperature and its application on electrode materials with large volume changes.

Declaration of competing interest

The authors declare that they have no known competing financial interests or personal relationships that could have appeared to influence the work reported in this paper.

CRediT authorship contribution statement

Xiang Han: Writing - original draft, Funding acquisition. **Ziqi Zhang:** Investigation. **Songyan Chen:** Supervision, Funding acquisition, Writing - review & editing. **Yong Yang:** Supervision.

Appendix A. Supplementary data

Supplementary data to this article can be found online at https://doi.org/10.1016/j.jpowsour.2020.228245.

References

[1] M. Armand, J.-M. Tarascon, Building better batteries, Nature 451 (2008) 652–657.
[2] P. Simon, Y. Gogotsi, B. Dunn, Where do batteries end and supercapacitors begin? Science 343 (2014) 1210–1211.
[3] H. Tian, F. Xin, X. Wang, W. He, W. Han, High capacity group-IV elements (Si, Ge, Sn) based anodes for lithium-ion batteries, J. Materiomics 1 (2015) 153–169.
[4] X. Zuo, J. Zhu, P. Müller-Buschbaum, Y.J. Cheng, Silicon based lithium-ion battery anodes: a chronicle perspective review, Nano Energy 31 (2017) 113–143.
[5] L. Zhang, X. Liu, Q. Zhao, Si-containing precursors for Si-based anode materials of Li-ion batteries: a review, Energy Storage Mater. 4 (2016) 92–102.
[6] H. Chen, Z. Dong, Y. Fu, Silicon nanowires with and without carbon coating as anode materials for lithium-ion batteries, J. Solid State Electrochem. 14 (2010) 1829–1834.
[7] X. Han, H. Chen, J. Liu, A peanut shell inspired scalable synthesis of three-dimensional carbon coated porous silicon particles as an anode for lithium-ion batteries, Electrochim. Acta 156 (2015) 11–19.
[8] N. Liu, Z. Lu, J. Zhao, M.T. McDowell, H.W. Lee, W. Zhao, Y. Cui, A pomegranate-inspired nanoscale design for large-volume-change lithium battery anodes, Nat. Nanotechnol. 9 (2014) 187–192.
[9] L.F. Cui, Y. Yang, C.M. Hsu, Carbon−silicon core−shell nanowires as high capacity electrode for lithium ion batteries, Nano Lett. 9 (2009) 3370–3374.
[10] X. Zhang, D. Kong, X. Li, Dimensionally designed carbon–silicon hybrids for lithium storage, Adv. Funct. Mater. 29 (2019) 1806061.
[11] F.M. Hassan, R. Batmaz, J. Li, X. Wang, X. Xiao, A. Yu, Z. Chen, Nat. Commun. 6 (2015) 8597.
[12] T. Ma, H. Xu, X. Yu, H. Li, W. Zhang, X. Cheng, X. Qiu, Lithiation behavior of coaxial hollow nanocables of carbon–silicon composite, ACS Nano 13 (2019) 2274–2280.
[13] B.J. Chen, L.H. Zu, Y. Liu, R.J. Meng, Y.T. Feng, C.X. Peng, F. Zhu, T.Z. Hao, J. J. Ru, Y.G. Wang, J.H. Yang, Space-confined atomic clusters catalyze superassembly of silicon nanodots within carbon frameworks for use in lithium-ion batteries, Angew. Chem. 132 (2020) 3161–3166.
[14] Q.B. Zhang, H.X. Chen, L.L. Luo, B. Zhao, H. Luo, X. Han, W. Jiang, C.M. Wang, Y. Yang, T. Zhu, M.L. Liu, Harnessing the concurrent reaction dynamics in active Si and Ge to achieve high performance of lithium-ion batteries, Energy Environ. Sci. 11 (2018) 669–681.
[15] B. Wang, X. Li, X. Zhang, B. Luo, Y. Zhang, L. Zhi, Contact-engineered and void-involved silicon/carbon nanohybrids as lithium-ion-battery anodes, Adv. Mater. 25 (2013) 3560–3565.
[16] I.H. Son, J.H. Park, S. Kwon, Silicon carbide-free graphene growth on silicon for lithium-ion battery with high volumetric energy density, Nat. Commun. 6 (2015) 7393.
[17] L. Li, Z. Zuo, H. Shang, In-situ constructing 3D graphdiyne as all-carbon binder for high-performance silicon anode, Nano Energy 53 (2018) 135–143.
[18] S. Piscanec, M. Cantoro, A.C. Ferrari, Raman spectroscopy of silicon nanowires, Phys. Rev. B 68 (2003) 241312.
[19] Z. Ni, Y. Wang, T. Yu, Raman spectroscopy and imaging of graphene, Nano Res. 1 (2008) 273–291.
[20] T. Liu, Q. Tian, W. Zhang, J. Chen, L. Yang, Fe_xO_y nanoparticles in-situ embedded in porous carbon framework towards improved lithium storage, Mater. Chem. Phys. 227 (2019) 12–20.
[21] C.X. Peng, H.X. Chen, Q.Y. Li, W.W. Cai, Y. Qin, Q.S. Wu, J.H. Yang, Y. Yang, Synergistically reinforced lithium storage performance of in-situ chemically grown Silicon@Silicon oxide core-shell nanowires on three-dimensional conductive graphitic scaffolds, J. Mater. Chem. A 2 (2014) 13859–13867.
[22] S. Kim, J. Ihm, H.J. Choi, Y.W. Son, Origin of anomalous electronic structures of epitaxial graphene on silicon carbide, Phys. Rev. Lett. 100 (2008) 176802.
[23] P. Kostestkyy, J. Yu, R.J. Gorte, Structure–activity relationships on metal-oxides: alcohol dehydration, Catal. Sci. Technol. 4 (2014) 3861–3869.
[24] H. Slosiariková, J. Bujdák, V. Hlavatý, IR spectra of octadecylammonium-montmorillonite in the range of the Si-O vibrations, J. Inclusion Phenom. Mol. Recognit. Chem. 13 (1992) 267–272.
[25] Y. Song, T. Sakurai, K. Kishimoto, Optical and structural properties of low-temperature PECVD ETMS SiO_x thin films, Thin Solid Films 334 (1998) 92–97.
[26] X.Q. Yang, J. McBreen, W.S. Yoon, Structural studies of the new carbon-coated silicon anode materials using synchrotron-based in situ XRD, Electrochem. Commun. 4 (2002) 893–897.
[27] D. Shen, C. Huang, L. Gan, Rational design of Si@SiO$_2$/C composites using sustainable cellulose as a carbon resource for anodes in lithium-ion batteries, ACS Appl. Mater. Interfaces 10 (2018) 7946–7954.
[28] J. Cho, Porous Si anode materials for lithium rechargeable batteries, J. Mater. Chem. 20 (2010) 4009–4014.
[29] Y. Li, K. Yan, H.W. Lee, Growth of conformal graphene cages on micrometre-sized silicon particles as stable battery anodes, Nat. Energy 1 (2016) 1–9.
[30] M.S. Wang, G.L. Wang, S. Wang, In situ catalytic growth 3D multi-layers graphene sheets coated nano-silicon anode for high performance lithium-ion batteries, Chem. Eng. J. 356 (2019) 895–903.
[31] P. Nie, Z. Le, G. Chen, Graphene caging silicon particles for high-performance lithium-ion batteries, Small 14 (2018) 1800635.

[32] X. Ding, X.X. Liu, Y. Huang, Enhanced electrochemical performance promoted by monolayer graphene and void space in silicon composite anode materials, Nano Energy 27 (2016) 647–657.

[33] L. Zhang, W. Hao, H. Wang, Porous graphene frame supported silicon@ graphitic carbon via in situ solid-state synthesis for high-performance lithium-ion anodes, J. Mater. Chem. 1 (2013) 7601–7611.

[34] F. Tang, W. Zhou, M. Chen, J. Chen, J. Xu, Flexible free-standing paper electrodes based on reduced graphene oxide/δ-NaxV$_2$O$_5$· nH$_2$O nanocomposite for high-performance aqueous zinc-ion batteries, Electrochim. Acta 328 (2019) 135137.